Polymer electrolyte fuel cell stack modelling with temporal-spatial and EIS experimental validations[×]

Fei Gao [1], El-Hassane Aglzim [1], Benjamin Blunier [1], Abdellatif Miraoui [1] and Amar Rouane [2]

[1] University UTBM, Systems and Transport Laboratory, Rue Ernest Thierry Mieg, Belfort, France
[2] University of Nancy, Electronic Instrumentation Laboratory of Nancy, Bd des Aiguillettes, Vandoeuvre-les-Nancy, France.

Abstract

This paper concerns two basic issues of fuel cell research: modelling and experimental validation. In particular, the EIS method (Electrochemical Impedance Spectroscopy) is applied to a PEMFC (Proton Exchange Membrane Fuel Cell). The experiments have been performed using a low-cost test bench and instrumentation developed around a 1200W Nexa fuel cell.
A multi-physical dynamic model for PEM fuel cell (PEMFC) stack is described. The 1-D dynamic PEMFC stack model covers 3 major fuel cell physical domains: electrical, fluidic and thermal. The model is capable to predict the accuracy stack profiles in time and space scales. The model has been validated with different experimental tests: temporal, spatial and impedance spectroscopy method.

An impedance spectroscopy at low frequencies analysis has been performed. The experimental and simulated Nyquist plots show that the dynamic behavior of the fuel cell stack can be well predicted by the proposed fuel cell stack model. Comparison between experimental and model impedance results is studied and a similitude between the two Nyquist plots in high frequencies can be founded.

1. Introduction

Over last 20 years, research and development studies about fuel cells have been done increasingly because of the demand of developing an effective and no pollutant system. Such a system can provide energy in some sectors such as transportation (car, bus, boats, submarines, etc…), portable (communication, computers, etc…) and stationary (generation of electricity and heat for the schools, buildings, etc…) [1, 2].

PEM fuel cell is an electrochemical device that combines hydrogen and oxygen, with the aid of electrocatalysts, to produce electricity. It consists of two electrodes: one, negatively charged (anode), in which the hydrogen oxidation takes place and another, positively charged (cathode), where the oxygen reduction occurs. Between the electrodes there is an electrolyte (thin ion-conducting polymeric membrane) which allows proton to move from the anode to the cathode, but blocks electrons and forces them to pass through the external load [3].

The fuel cell is a reliable and sustainable way to produce environmentally friendly energy for many applications. The PEM fuel cell is considered as the most promising technology for transportation and portable applications because of the low operating temperature and ease of assembly [4].
However, some problems still posed and slow down the development of the fuel cell for civil applications.

In order to improve fuel cells performances and to increase their lifetime, it is necessary to perform suitable measurements like EIS [5,6,7]. EIS analysis is important for a better comprehension of physico-chemical phenomena taking place in PEMFCs, for optimization in their components (membrane, electrode, flow fields . . .) and in their operating conditions as well.

[×] Presented at the MODVAL7 symposium, Morges / Switzerland, March 2010

This purpose is experimentally accomplished with EIS technique and using the equivalent circuit description for parameters determination [8].

For this reasons, in following sections firstly a dynamic fuel cell model described in VHDL-AMS is presented. Then the test bench used for EIS measurement is described. Finally, a comparison between experimental and model results is reported.

2. Fuel cell dynamic modelling

In this section, a fuel cell multi-physical dynamic model is presented. The model divides one single cell into 8 layers based on their geometries and functionalities. Each individual layer is associated with different physical equations in 3 physical domains: electrical, fluidic and thermal. The combination of these layers gives a complete single cell model. Furthermore, the stack model can be obtained from the combination of the single cell model.

2.1 Fluid channels layer modelling (cooling layer, cathode and anode channel layers)

The reactant gases are supplied to the electrochemical reaction site by fluid channels during operating. In addition to the cathode channels and anode channels, cooling channels can be found in the fuel cell, especially for large fuel cell stack. These channels are usually included in solid materiel layers (metal or graphite). These layers form the bipolar plate of the fuel cell.

2.1.1 Electrical domain:

The bipolar plate has its electrical resistance. This resistance is relatively small compare to the membrane resistance during the fuel cell operating. Thus, this resistance can be neglected. The voltage drop through the bipolar plate can be assumed to zero:

$$U_{ch} = 0 \tag{1}$$

Where U_{ch} represents the voltage contribution of channels layer to the cell voltage (V).

2.1.2 Fluidic domain:

The fluidic dynamic response of a fuel cell is generally due to the gas pressure dynamics in the fuel cell channels (cooling, cathode and anode) which are given by the mass balance equation:

$$\frac{M_{gas} \cdot V_{Ch}}{R \cdot T}\left(\frac{d}{dt} P_{Ch}\right) = q_{inlet} + q_{outlet} + q_{GDL} \tag{2}$$

where V_{ch} is the volume of the channels (m^3), M_{gas} the specific gas molar mass (kg/mol), P_{ch} the specific gas pressure in the channels (Pa), q_{inlet} the fluid mass flow (kg/s) entering the channels, q_{outlet} the fluid mass flow (kg/s) leaving the channels and q_{GDL} the fluid mass flows (kg/s) from gas diffusion layer (O_2, N_2, H_2, H_2O).
Assuming the flow in the channels is laminar, the wall friction loss (pressure drop) in the gas channels can be modeled by Darcy-Weisbach Equation [9]:

$$\Delta P = 32 \cdot \frac{\mu_{gas} \cdot L \cdot V_S}{\left(D_{hydro}\right)^2} \tag{3}$$

Where D_{hydro} is the channel hydraulic diameter (m), V_s the mean fluid velocity in the channels (m/s), L the length of the channel (m) and μ_{gas} the gas dynamic viscosity (Pa.s) in the channel.
The gas fluid velocity can be obtained as follow:

$$V_s = \frac{q_{inlet} + q_{outlet}}{2 \cdot \rho_{ch} \cdot S_{ch}} \tag{4}$$

Where ρ_{ch} is the channels gas mean density (kg/m^3) and S_{ch} the channels section area (m^2).

2.1.3 Thermal domain:

The thermal dynamic in the channels can be separated to 2 different control volumes: solid portion (support bipolar plate) and gas portion (gas in the channels).
The dynamic energy balance in 2 control volumes can be described:

$$\left(\rho_{CV} \cdot V_{CV} \cdot C_{p,CV}\right)\frac{dT_{CV}}{dt} = \underbrace{\dot{Q}_{cond}}_{\text{conduction}} + \underbrace{\dot{Q}_{forced\_conv}}_{\text{forced convection}} + \underbrace{\dot{Q}_{nat\_conv\_radia}}_{\text{natural convection } and \text{ radiation}} + \underbrace{\dot{Q}_{mass}}_{\text{convective mass flow}} \quad (5)$$

Where T_{CV} is the corresponding volume temperature (K), ρ_{CV} the corresponding volume density (kg/m^3), V_{CV} the corresponding volume (m^3), $C_{p,CV}$ the corresponding volume thermal capacity (J/kg·K) and $\dot{Q}_{()}$ the different heat flow in and out from the control volume (J/s).
The conduction heat flow can be modeled by Fourier law [10]:

$$\dot{Q}_{cond} = \frac{\lambda \cdot S}{\delta}\Delta T \quad (6)$$

Where λ is the material thermal conductivity (W/m·K), S the contact area (m^2) and δ the material thickness (m).
The forced convection heat flow, such as cooling flow, cathode and anode flow, can be described by the Newton cooling law [2]:

$$\dot{Q}_{forced\_conv} = h_{forced} \cdot S_{contact} \cdot (T_{fluid} - T_{solid}) \quad (7)$$

where h_{forced} is the forced convection heat transfer coefficient (W/m^2·K).
The heat exchanges due to the natural convection and radiation can be described by the same law:

$$\dot{Q}_{nat\_conv\_radia} = h_{nat\_radia} \cdot S_{ext} \cdot (T_{amb} - T_{solid}) \quad (8)$$

Where h_{nat_radia} is the combined natural convection and radiation heat transfer coefficients (W/m^2·K), and T_{amb} is the external environment temperature (K).
When the fuel cell stack is operating, different fluid flow entering or leaving the layer brings or remove the heat from the layers. These convective mass transports bring the additional heat flow:

$$\dot{Q}_{mass} = \left[\sum_{fluid}\left(q_{fluid} \cdot C_{p,fluid}\right)\right] \cdot \left(T_{fluid} - T_{layer}\right) \quad (9)$$

2.2 Gas diffusion layer modelling (cathode and anode gas diffusion layers)

In order to have a uniform distribution of gas during the electrochemical reaction, the gas supplied from channels should pass a thin diffusion layer before reaches to the reaction site. These layers, who are generally known as “gas diffusion layer (GDL)”, have porous structure for the gas pass through and for the produced water evacuation.

2.2.1 Electrical domain:

The gas diffusion layer is usually made by carbon paper or tissue, the thickness of this layer is in order of hundreds micro meter. Thus the electrical resistance of this layer in the model can be neglected. The voltage drop in these layers (cathode and anode) can be assumed to zero:

$$U_{GDL} = 0 \quad (10)$$

Where U_{GDL} is the gas diffusion layer voltage contribution to the cell voltage (V).

2.2.2 Fluidic domain:

The multi-gas diffusions (O_2, N_2, H_2O at cathode and H_2, H_2O at anode) through gas diffusion layers can be described by Stefan-Maxwell equation [11]:

$$\Delta P_a = \frac{\delta_{GDL} \cdot R \cdot T}{P_{tot} \cdot S} \sum_{b \neq a} \frac{P_a \cdot \frac{q_b}{M_b} - P_b \cdot \frac{q_a}{M_a}}{D_{ab}} \tag{11}$$

Where ΔP_a is the individual pressure drop of specie a through gas diffusion layer, δ_{GDL} the diffusion layer thickness (m), S is the cell section area (m^2), P_{tot} is the mean gas total pressure (Pa) in the diffusion layer, $M_{()}$ is the gas molar mass (kg/mol), b stands for species other than species a, and D_{ab} is the binary diffusion coefficient between the species a and b (m^2/s).

2.2.3 Thermal domain:

Due to the thickness of gas diffusion layers, the natural convections in these layers can be neglected. The dynamic energy balance in gas diffusion layers can be obtained:

$$\left(\rho_{GDL} \cdot V_{GDL} \cdot C_{p,GDL}\right) \frac{dT_{GDL}}{dt} = \underbrace{\dot{Q}_{cond}}_{\text{conduction}} + \underbrace{\dot{Q}_{mass}}_{\substack{\text{convective} \\ \text{mass flow}}} \tag{12}$$

2.3 Catalyze layer modelling (cathode and anode catalyst layer)

The electrochemical reactions in fuel cell are occurred in these layers. These layers have three phase contact area (reactant gas, catalyze and electrolyte), in which the electrochemical reaction takes place.

2.3.1 Electrical domain:

The catalyze layers are the places where the electrochemical reactions are occurred. The reactions generate the electromotive force in these layers. The cathode and anode electromotive force E_{emf} (V) can be obtained from Nernst equation [12]:

$$E_{emf} = E_0 - \beta(T - T_c) + \frac{R \cdot T}{2F} \ln\left(\sqrt{P_{O_2}} \cdot P_{H_2}\right) \tag{13}$$

Where $E_0 = 1.229$ is the reaction electromotive force in standard condition (V), $T_c = 298.15$ the temperature offset of correction (K), $\beta = 0.85 \cdot 10^{-3}$ the correction coefficients, T the temperature of cell (K), $R = 8.31$ the gas constant (J/(mol·K), $F = 96485$ the Faraday constant (C/mol), and P_{O_2}, P_{H_2} the pressures of oxygen (atm) and of hydrogen (atm), respectively.

In addition to this electromotive force, the dynamic voltage drop generally know as "activation loss" U_{act} (V) due to the cell current when operating and double layer capacity in these layers can be modelled by Tafel equation [13] and first order dynamic system:

$$\frac{d}{dt} U_{act} = \frac{i}{C_{dl}} \left(1 - \frac{\alpha \cdot n \cdot F}{R \cdot T \ln\left(\frac{i}{i_0 \cdot S}\right)} U_{act} \right) \tag{14}$$

Where i is the cell current (A), C_{dl} the cell double layer capacity (F), n the number of electrons involved in the reaction, α the symmetry factor, S the cell section area (m^2) and i_0 the cell exchange current (A).

The catalyze layers overall voltage contribution to the cell voltage U_{cata} (V) can be then obtained:

$$U_{cata} = E_{emf} - U_{act} \tag{15}$$

2.3.2 Fluidic domain:

The gas mass flow rates in catalyze layers are directly related to cell current i, these mass flows can be obtained by following equations:

$$q_{O_2} = \frac{M_{O_2} \cdot i}{4F} \tag{16}$$

$$q_{H_2} = \frac{M_{H_2} \cdot i}{2F} \tag{17}$$

$$q_{H_2O,produced} = \frac{M_{H_2O} \cdot i}{2F} \tag{18}$$

In addition, the water mass flow $q_{H_2O,net}$ from membrane through catalyze layer to diffusion layer is related to the membrane water content, this mass flow can be found in the membrane modeling section.

2.3.3 Thermal domain:

The catalyze layers thermal dynamic equations can be described as:

$$\left(\rho_{CV} \cdot V_{CV} \cdot C_{p,CV}\right)\frac{dT_{CV}}{dt} = \underbrace{\dot{Q}_{cond}}_{\text{conduction}} + \underbrace{\dot{Q}_{mass}}_{\substack{\text{convective} \\ \text{mass flow}}} + \underbrace{\dot{Q}_{sources}}_{\text{internal source}} \tag{19}$$

The additional internal heat source is due to the irreversible losses at the cathode catalyst layer due to entropy change in the reaction and the activation losses. These heat sources can be expressed:

$$\dot{Q}_{sources} = \underbrace{-i \cdot \frac{T \cdot \Delta S}{2F}}_{\text{entropy change part}} + \underbrace{i \cdot U_{act}}_{\text{activation part}} \tag{20}$$

Where ΔS is the entropy change (J/mol·K) during the electrochemical reaction.

2.4 Membrane layer modelling (membrane layer)

In PEM fuel cell, the membrane layer is the path for proton transportation from anode to cathode. The proton conduction is only possible if the membrane is hydrated. Thus, the water balance in the membrane is very important for the fuel cell performance.

2.4.1 Electrical domain:

The voltage drop in membrane layer is due to the membrane electrical resistance. The membrane resistance is highly related to its water content, the membrane resistance increase when the water content decrease. In addition, the local resistance in the membrane is not uniform. This is because the water distribution in membrane is not uniform during the cell operating.

Thus, the total membrane voltage contribution to the cell voltage U_{mem} (V) can be obtained:

$$U_{mem} = -R_{mem} \cdot i = -\frac{i}{S}\int_0^{\delta mem} r(T,\lambda(z))dz \tag{21}$$

Where R_{mem} is the membrane total resistance (Ω), $r(T,\lambda(z))$ the local resistively of membrane (Ω·m) in function of cell temperature T (K) and membrane local water content $\lambda(z)$, δ_{mem} the membrane thickness (m) and z the membrane water diffusion axis direction.

The local resistively of the membrane can be obtained by following equation [6]:

$$r = \begin{cases} \dfrac{e^{\left[1268\cdot\left(\frac{1}{T}-\frac{1}{303}\right)\right]}}{0.1933} & if \;\; 0 < \lambda(z) \le 1 \\ \dfrac{e^{\left[1268\cdot\left(\frac{1}{T}-\frac{1}{303}\right)\right]}}{0.5193\cdot\lambda(z) - 0.326} & if \;\; \lambda(z) > 1 \end{cases} \tag{22}$$

2.4.2 Fluidic domain:

The membrane local water content can be modelled by following equations [14]:

$$\lambda(z) = \begin{cases} 0.0043 + 17.81 \cdot a_{H_2O} - 39.85 \cdot a_{H_2O}^2 + 36 \cdot a_{H_2O}^3 & \text{if } 0 < a_{H_2O} \leq 1 \\ 14 + 1.4 \cdot (a_{H_2O} - 1) \quad \text{if } 1 < a_{H_2O} \leq 3 \end{cases} \tag{23}$$

Where a_{H_2O} is the water activity, defined from water partial pressure P_{H_2O} (Pa) and water saturation pressure P_{sat} (Pa):

$$a_{H_2O} = \frac{P_{H_2O}}{P_{sat}} \tag{24}$$

The water balance in the membrane layer can be described by two different phenomenons: the *electro-osmosis* phenomenon described by equation (25), and the *back diffusion* phenomenon described by equation (26) [15]:

$$J_{drag} = \frac{n_{sat}}{11} \cdot \lambda(z) \cdot \frac{i}{2F} \cdot M_{H_2O} \tag{25}$$

$$J_{back\_diff} = \frac{\rho_{dry}}{M_n} \cdot D_\lambda \cdot \frac{d\lambda(z)}{dz} \cdot S \cdot M_{H_2O} \tag{26}$$

Where $n_{sat} = 22$ is the electro-osmotic drag coefficient for maximum hydration condition, ρ_{dry} the dry density of the membrane (kg/m^3), D_λ the mean water diffusion coefficient in the membrane (m²/s) and M_n the equivalent mass of the membrane (kg/mol).

The water diffusion coefficient D_λ can be obtained by an empirical formula [9]:

$$D_\lambda = 10^{-4} \cdot e^{\left(2416 \cdot \left(\frac{1}{303} - \frac{1}{T}\right)\right)} \cdot \begin{cases} 10^{-6} & \text{if } \lambda(z) < 2 \\ 10^{-6} \cdot (1 + 2(\lambda(z) - 2)) & \text{if } 2 \leq \lambda(z) \leq 3 \\ 10^{-6} \cdot (3 - 1.67(\lambda(z) - 3)) & \text{if } 3 < \lambda(z) < 4.5 \\ 1.25 \cdot 10^{-6} & \text{if } \lambda(z) \geq 4.5 \end{cases} \tag{27}$$

Thus, the overall mass flow in the membrane can be obtained by adding the two opposite phenomenon flow rate together:

$$q_{H_2O,net} = J_{drag} + J_{back\_diff} \tag{28}$$

The equation (28) is a differential equation of $\lambda(z)$ and can be solved to analysical results.

2.4.3 Thermal domain:

The membrane thermal dynamic can be described by following equations:

$$\left(\rho_{CV} \cdot V_{CV} \cdot C_{p,CV}\right) \frac{dT_{CV}}{dt} = \underbrace{\dot{Q}_{cond}}_{\text{conduction}} + \underbrace{\dot{Q}_{mass}}_{\substack{\text{convective} \\ \text{mass flow}}} + \underbrace{\dot{Q}_{joule}}_{\text{resistive heat}} \tag{29}$$

During the fuel cell operating, the membrane has an additional heat term due to the membrane resistance and cell current (Joule effect). This heat source can be modeled quite simply:

$$\dot{Q}_{joule} = i^2 \cdot R_{mem} \tag{30}$$

1.5. Fuel cell model experimental results

2.5.1 Model temporal domain validations

The model presented in the previous section is validated temporally at first. The model is calibrated to a commercial Ballard Nexa 1.2 kW fuel cell stack. This stack has 47 individual cells and the stack is cooled by air fan. The model results are shown in the figures below.

Figure 1 presents the stack voltage profile. A step current of 28 A during 730 s is used for real stack and the presented model.
The stack voltage response from the Ballard Nexa stack and the model can be found in Figure 2. The entire stack model voltage response shows a very good dynamic accuracy compare to the experimental results. The maximum voltage error is less than 1 V, which present a relative error less than 5 % in voltage.
It should be noted that, each cell in the stack is modeled individually: these cell model has the same physical equations that described previously, but in the model they do not have the same boundary conditions, such as gas pressure or temperature. Thus the model itself can describe the spatial distribution of physicals in the stack.
Figure 3 shows the individual cell temperature at 350 s in stack from the model computations. The spatial cell temperature prediction has a great agreement to the experimental data.
Furthermore, the entire stack temperature spatial and temporal evolution during the stack operating is shown in Figure 4. The non uniform temperature distribution in the stack can be seen clearly.

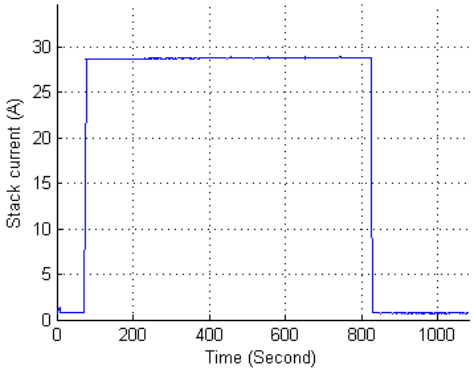

Figure 1 : Stack current

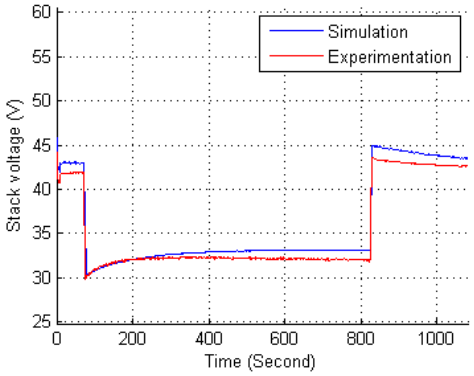

Figure 2 : Stack voltage

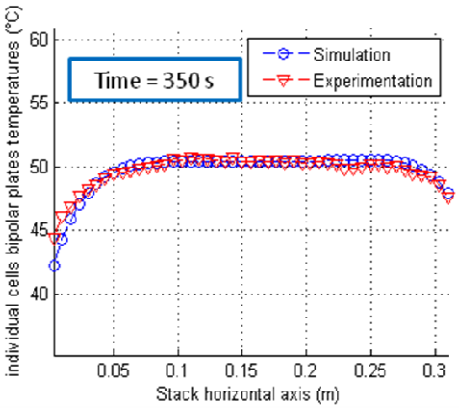

Figure 3 : Individual cell temperature

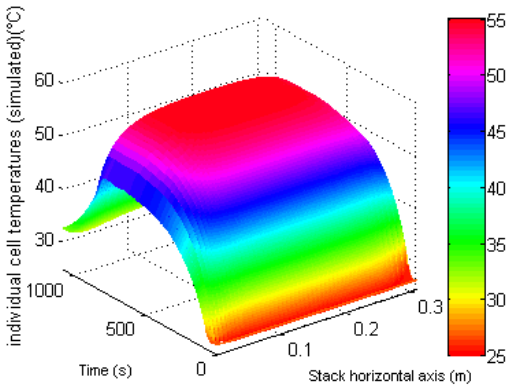

Figure 4 : Cells temperature evolution

3. Impedance Measurement – EIS technique

In this section, the test bench used for the impedance measurement is presented. Complex impedance was carried out on a PEM fuel cell using the EIS technique.
Experimental results are presented and commented. The tests are performed on a 1200W PEM Fuel cell with system controller and electronic devices at different current levels.

3.1. The Nexa fuel cell and the testbench description

A Ballard PEM stack (Nexa power module), shown in figure 5, was used in this work, providing 1200 watts of unregulated DC power at a nominal output voltage of 26 VDC, its output current can reach 44A and voltage usually up to 42V.
It's composed of 47 individual cells and has a central controller, air compressor and other electrical devices which consume electric power from the fuel cell stack, making the accurate EIS measurement more difficult.

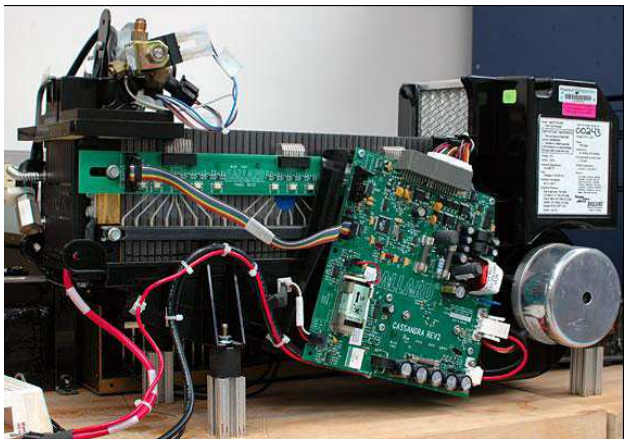

Figure 5 : The Ballard PEM stack (1200W fuel cell)

The experimental test bench used for the complex impedance measurement is shown in Figure 6.
It included the fuel cell, the electronic load and the frequency generator, and it's working in galvanostatic impedance mode.
The sinusoidal current signal applied to the fuel cell through the electronic load modulates the current from the fuel cell stack by using the Electrochemical Impedance Spectroscopy method (description in the part 2).
The measurement test bench is used to acquire the voltage and current waveform data in time domain. The current information at the electronic load is sent to the computer. The fuel cell voltage is measured by the electronic load directly on the fuel cell.

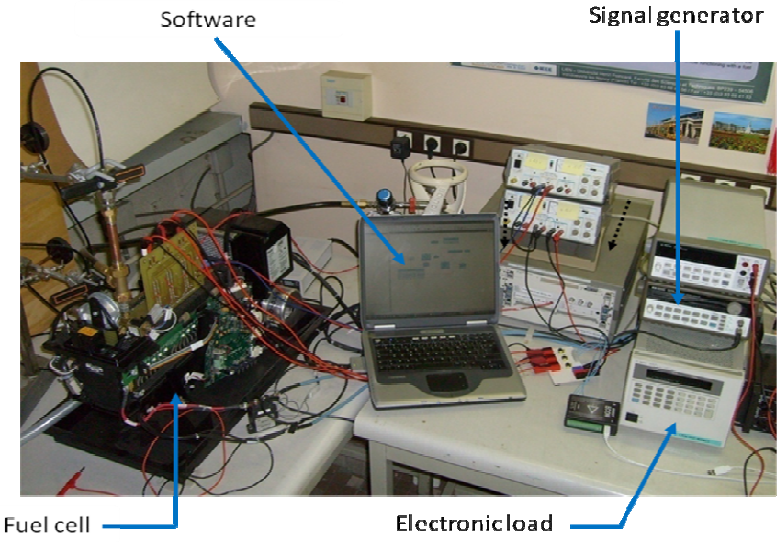

Figure 6 : The impedance measurement testbench

The voltage and the current data are read back, via GPIB (General Purpose Interface Bus) to a computer. And then stored and processed. In particular, a FFT algorithm (Fast Fourier Transform) is applied in order to represent voltage and current in frequency domain. Thus, simply dividing the transformed voltage by the transformed current, it is possible to obtain complex impedance (both magnitude and phase) at the desired frequency.
This procedure can be repeated at any frequency within the capabilities of the adopted equipment, resulting in a full spectrum impedance measurement, useful in fuel cell EIS studies. This technique is a powerful technique that can provide a lot of information in a short period of time and has been applied to proton exchange membrane fuel cell (PEMFC) in a number of recent studies [16].
The small excitation waveforms of this amplitude caused only minimal perturbation of the fuel cell system and reduced errors caused by the measurement technique. The level of noise in the impedance data depends on the size of current and voltage signals returned to the control and treatment program.
Due to electronic load limit power, than cannot exceed 600 W, the impedance measurements were carried out for a current range from 1 A to 10 A, in steps of 1 A.

3.2 – Experimental results

Impedance tests were performed on the fuel cell stack with system controller and electronic devices at different current levels.
The frequency range of the spectrum goes from 8 mHz to 12.4 kHz**,** and there are 10 frequencies taken for each decade. The applied current excitation is such as to produce a voltage oscillation of about 1V peak-to-peak (essential requirement to eliminate disturbances due to the system controller of the fuel cell). Besides one complete measurement took about 45 minutes, because it has been employed the single-sine technique [17]
The current range goes from 1 A to 10 A by step of 1 A. This limit is due to power limit of the electronic load that can reached only 600 W.
Figure 7 shows the experimental results of the impedance measurement for the current range defined previously. The impedance is represented in Nyquist diagrams.

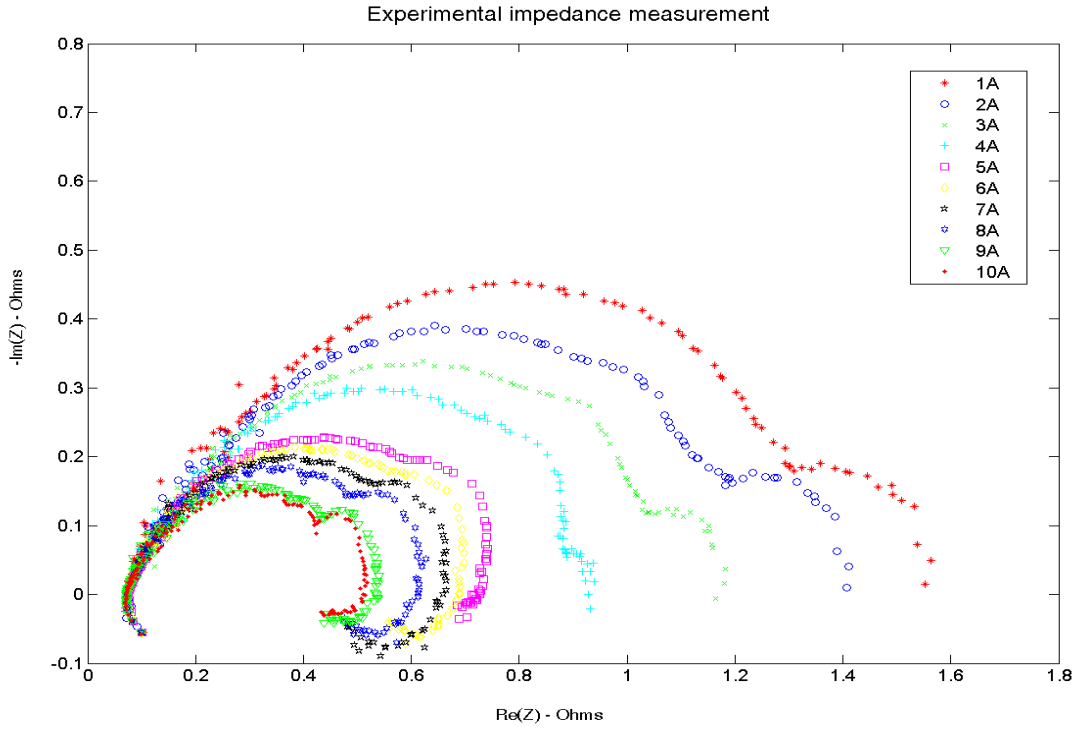

Figure 7 : Experimental results carried out with the test bench

The impedance in the frequency range is represented by two lobes. The activation losses (i.e. the resistance of polarization) are extremely high, because a temperature of 36 °C is relatively low temperature for the operation of the PEM fuel cell. The polarization resistance is the sum of the activation

losses of the anode and the cathode. This resistance increases in numbers of cell, which is the sum of each polarization resistance of the whole of the cells. Ohmic resistance does not vary; it is constant for the different current.

The reader may note that for a current of 5 A, the appearance of an inductor at low frequencies and that, for currents from 5 A to 10 A. For the high frequencies, we can note the appearance of an inductance due to the measure wires. The polarization resistance decreases when current increasing. It is of 1.477 Ω for 1 A and 0.425 Ohms for 10 A.

4. Comparison between experimental and model impedance results

To validate the dynamic of the fuel cell model described in the section 2, an impedance measurement was performed by the application of a current profile on the model and by using EIS technique. The current profile is the same that was used for experimental tests. Model results were compared to the experimental impedance results. The tests were performed for a current range from 1A to 10A. The current profiles were generated by Matlab with a rest period of 600s to allow the fuel cell to stabilize in temperature.

Due to simulation time, we have a limited frequency range of 8 mHz to 15.625 Hz.

Figure 8 shows the impedance results that we have obtained in simulation and the comparison with those obtained by experimentation.

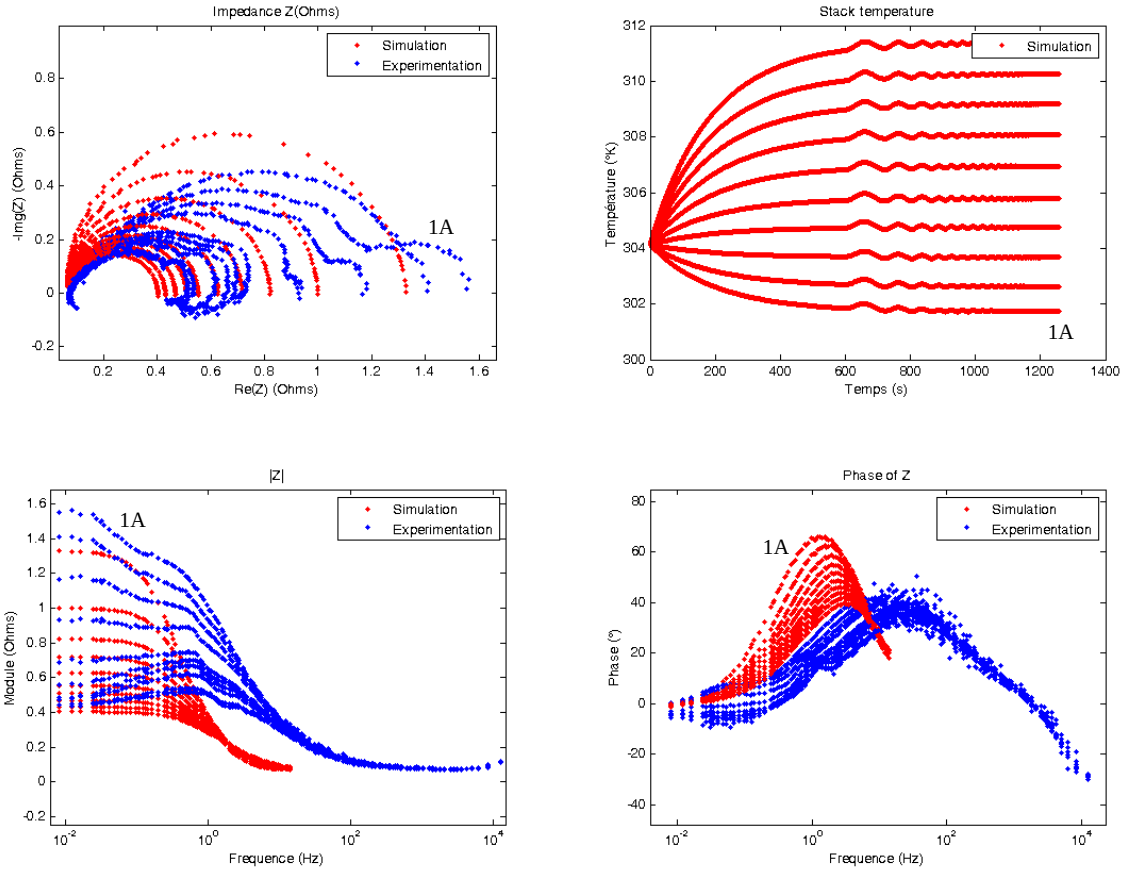

Figure 8: Model and experimental impedance results

A similitude between the two graphs (experimental and simulation) in high frequencies can be seen.
At low frequencies, the two curves are not identical, probably due to the experimental conditions that are not the same with the model experiment.

The model doesn't integrate the anode side of the fuel cell. This is why the second lobe doesn't appear in the Nyquist plot.
The experimental and simulated Nyquist plots show that the dynamic behavior of the fuel cell stack can be well predicted by the proposed fuel cell stack model

5. Conclusion

The present paper deals with the modelling and the EIS validation for a PEM fuel cell. The modeling and the experimental validation was done on a 1200W Nexa fuel cell from Ballard Company.

A multi-physical dynamic model for the Nexa fuel cell was firstly presented. The model is capable to predict the accuracy stack profiles in time and space scales.
In addition of the temporal model validation, an impedance spectroscopy at low frequencies analysis has been performed with an experimental test bench and with the 1D model.
By varying the current profiles, EIS data have been considered in order to observe the impedance modulus behavior at low and high frequency. Studying these impedance variations, as shown in this paper, it will be possible to determine the physical-chemical phenomena taking place in PEMFCs.
The experimental and simulated Nyquist plots show that the dynamic behavior of the fuel cell stack can be well predicted by the proposed fuel cell stack model. Comparison between experimental and model impedance results shows a similitude between the two Nyquist plots in high frequencies.

6. References:

[1] S. Gottesfeld, T.A. Zawodiznski, in: R.C. Alkire, H. Gerischer, D.M. Kolb, C.W. Tobias (Eds.), *Advances in Electrochemical Science and Engineering*, vol. 5, John Wiley and Sounds, Inc., New York, 1997, p. 195.

[2] NR. Wagner, in: E. Barsoukov, J.R. Macdonald (Eds.), *Impedance Spectroscopy - Theory, Experiment, and Applications*, second ED., John Wiley & Sounds, Inc., Hoboken, New Jersey, 2005, p. 496.

[3] Lee J.H., Lalk T.R. and Appleby A.J., *Modeling electrochemical performance in large scale proton exchange membrane fuel cell stacks*, Journal of Power Sources Vol 70, pp.258-268 (1998)

[4] R.A. Lemons, *Fuel Cells for transportation*, 29, Journal of Power Sources, Issues 1-2, January 1990, p. 251-264.

[5] Romero-Castanon T., Arriaga LG., Cano-Castillo, *Impedance spectroscopy as a tool in the evaluation of MEA*, Journal of Power Sources 1 18 (1-2): 179-1 82 (2003)

[6] Ciureanu M., Roberge R., *Electrochemical impedance study of PEM fuel cells. Experimental diagnostics and modeling of air cathodes*, Journal of Phisycal Chemistry, B 105 (17): 3531-3539 (2001)

[7] B. Andreaus, G. Scherer, *Interpretation of current-voltage characteristics of polymer electrolyte fuel cells by impedance spectroscopy*, The Fuel Cell World, Conference Proceedings, Lucerne, Switzerland (2002)

[8] Balkin A.R., *Modelling a 500W polymer electrolyte membrane fuel cell*, A 12 Credit Point Project submitted in partial fulfillment of the requirement for the Degree of Bachelor of Engineering

[9] F. M. White, *Fluid Mechanics*. 4th ed. 1998: McGraw Hill. 826.

[10] Incropera, DeWitt, Bergman, and Lavine, *Fundamentals of Heat and Mass Transfer*. 6e ed. Vol. 1. 2007: Wiley.

[11] D. M. Bernardi and M. W. Verbrugge, *Mathematical Model of a Gas Diffusion Electrode Bonded to a Polymer Electrolyte.* AIChE Journal, 1991. **37**(8): p. 13.

[12] J. Larminie and A. Dicks, *Fuel Cell Systems Explained*. 2e ed. 2003: Wiley.

[13] R. O'Hayre, S.-W. Cha, W. Colella, and F. B. Prinz, *Fuel cell fundamentals*. 1st ed. 2005: John Wiley & Sons, INC. 409.

[14] T. E. Springer, T. A. Zawodzinski, and S. Gottesfeld, *Polymer Electrolyte Fuel Cell Model.* J. Electrochem. Soc, 1991. **138**(8): p. 9.

[15] J. T. Pukrushpan, A. G. Stefanopoulou, and H. Peng, *Control of Fuel Cell Power Systems*. 2004.
[16] N. Wagner, W. Schnurnberger, B. Muller *and* M. Lang, *Electrochemical impedance spectra of solid-oxide fuel cells and polymer membrane fuel cells,* Electrochemical Acta, Vol43, No. 24, pp. 3785-3793, 1998
[17] Princeton Applied Research Application Note AC-3, *Electrochemical impedance measurements: instrumentation and techniques*, Electrochemical instrument group.